Journal of the Indian Society of Remote Sensing (July 2020) 48(7):1007–1020
https://doi.org/10.1007/s12524-020-01131-6

RESEARCH ARTICLE

Identification of Remote Sensing-Based Land Cover Types Combining Nearest-Neighbor Classification and SEaTH Algorithm

Jinling Zhao[1] · Yan Fang[1] · Mingmei Zhang[2] · Yingying Dong[3,4]

Received: 10 July 2019 / Accepted: 28 July 2020 / Published online: 6 August 2020

Abstract
The development of spaceborne remote sensing has greatly facilitated the land cover mapping at various spatial scales. Classification accuracy, however, is usually affected by the heterogeneous spectra of different land cover types for medium–low-spatial-resolution images. The study is aimed at improving the classification accuracy at a city scale by proposing a hierarchical classification method. Time-series Landsat-5 and Landsat-8 Operational Land Imager remote sensing images of 4 years were used as the classified images. A total of six first-class land cover types were determined, namely woodland, grassland, cropland, wetland, artificial surface and others. The object-based image analysis was chosen over pixel-based approaches. More specifically, the nearest-neighbor (NN) classification and SEparability and THresholds (SEaTH) algorithm were combined to produce a hierarchical classification method (NN-SEaTH). SEaTH algorithm was first used to extract the wetland after performing image segmentation in eCognition Developer. Then, the non-wetland was further classified to vegetation and non-vegetation by using a normalized difference vegetation index image. Finally, the other types were then obtained using the NN classification. To validate the proposed method, the NN classifier and NN-SEaTH method were compared. The proposed technique is shown to increase the overall accuracy (OA) and kappa coefficient (k) for the 4 years. The OA and k are, respectively, 96.46% and 0.9231, 96.63% and 0.9269, 96.88% and 0.9394, 95.22% and 0.9239 that are much larger than 88.13% and 0.7503, 88.83% and 0.7660, 88.64% and 0.7630, 87.33% and 0.7371 derived from the NN approach. The study provides a reference for medium-resolution-based land cover mapping by a hierarchical classification.

Keywords Land cover · Landsat-8 · Nearest-neighbor classification · Remote sensing · SEaTH

✉ Yingying Dong
dongyy@radi.ac.cn

1 National Engineering Research Center for Agro-Ecological Big Data Analysis & Application, Anhui University, Hefei 230601, China

2 Department of Geology and Surveying and Mapping, Shanxi Institute of Energy, Jinzhong 030600, China

3 Key Laboratory of Digital Earth Science, Institute of Remote Sensing and Digital Earth, Chinese Academy of Sciences, Beijing 100094, China

4 Aerospace Information Research Institute, Chinese Academy of Sciences, Beijing 100094, China

Introduction

The environmental crises facing the Earth have to be considered such as cropland loss, soil erosion, water pollution, forest destruction, with increasing population size. It is of great significance to dynamically monitor and estimate the various Earth resources at regional/local, national, continental and global scales. Land cover/use is an important parameter to describe and reflect the influences caused by human activities (Foley et al. 2005), which is also the basis to understand the driving forces of land cover change (Lambin et al. 2001). Great attention has been paid to the identification of land cover information in different application fields. The greenhouse emissions from land-use change were estimated by using a worldwide agricultural model (Searchinger et al. 2008). The relationships of land use and the flow and water quality at both a regional scale and a local scale were examined by statistical and spatial analyses (Tong and Chen 2002). A dynamic inter- and intra-city analysis of spatial and temporal patterns of urban land-use change was carried out for rapidly developing cities with landscape pattern metrics (Seto and Fragkias 2005).

The above studies can be observed that land cover plays an important role in investigating the tempo-spatial dynamics of thematic objects. The development of remote sensing has provided a specific approach to derive the land cover information from various remotely sensed imageries, especially since the launches of the National Oceanic and Atmospheric Administration (NOAA) Advanced Very High-Resolution Radiometer (AVHRR), MODerate resolution Imaging Spectrometer (MODIS), Landsat series and Chinese Huanjing (e.g., HJ-1A/B/C), Ziyuan (e.g., ZY-3, ZY-3 02) and Gaofen series (e.g., GF-1, GF-2) (Loveland et al. 2000; Friedl et al. 2002; Chen et al. 2014; Gu and Tong 2015). Especially with a sharp increase in spatial resolution, more remotely sensed imagery and semi-automated/automated classification methods have been developed to improve the classification accuracies than traditional land cover mapping approaches (Singh and Garg 2014, 2015).

In addition, it can also provide cost-effective and accurate means to derive land resource information. For example, global, continental and national land cover datasets have been produced ranging from 1 km to 30 m based on various remote sensing imageries. The MODIS global land cover (GLC) product was generated at 1-km spatial resolution using supervised classification methodology and several classification systems, principally that of the IGBP (Friedl et al. 2002). The GLC2000 database has been produced at a spatial resolution of 300 m based on daily data from the VEGETATION sensor on-board SPOT 4 by an international partnership of 30 research groups coordinated by the European Commission's Joint Research Centre (Bartholome and Belward 2005). The GlobLand30 was produced at 30 m resolution using an approach based on the integration of pixel- and object-based methods with knowledge (POK) based on Landsat TM/ETM^{+} and HJ-1 satellite imagery 2010 (Chen et al. 2015).

It can be seen that most GLC products have been generally generated at a relatively large scale. The classification methodology mainly focuses on supervised classification or an integration of pixel- and object-based methods. Some specific classification methods are required when the study area is located in a city or a smaller region (Singh and Garg 2011, 2016). The identification accuracy and running speed are the two essential factors for remote sensing-based land cover classification, due to the large volume of time-series data. There are usually specific advantages and disadvantages for different methods. For example, nearest neighbor (NN) is easy to perform the classification procedures. The typical samples are just required to be selected after defining the feature space in eCognition (Trimble Navigation Ltd, Sunnyvale, California). Nevertheless, its processing speed is low when adding more feature variables in feature space and facing large-scale remote sensing data; this greatly affects the classification efficiency. Conversely, SEparability and THresholds (SEaTH) algorithm has a better performance in processing speed. The feature preference and optimal threshold can be easily determined, but it greatly relies on the Jeffries–Matusita (JM) distance. When the JM distance is greater than 1.80, the selected features and corresponding threshold values are generally satisfactory.

Summarizing the above studies, it can be concluded that it is highly necessary to improve the identification efficiency by combining or integrating different classification methods. In this study, a capital city was selected as the study area. Landsat-8 remotely sensed imagery was used as the data source for identifying land cover types, which has been proved to be the relatively satisfactory data. The hierarchical classification ideal was adopted according to the characteristics of specific land cover types. A combination method of NN classification and SEaTH algorithm was proposed to improve the identification accuracy of land cover at the city scale.

Materials and Methods

Study Area

Hefei, the capital city of Anhui Province, China, was selected as the study area. It is located in southeastern China, at longitudes ranging from 114° 54′ E to 119° 37′ E and latitudes ranging from 29° 41′ N to 34° 38′ N (Fig. 1). Specifically, Hefei has a subtropical monsoon climate with four distinct seasons. The average annual temperature is about 15.7 °C, with an average annual precipitation of 1000 mm and an average annual sunshine of 2100 h. The general trend of the urban terrain is high in the north, southeast and southwest, and low in central and southern areas.

Data Collection and Preprocessing

To validate the proposed classification method, four-year time-series remote sensing images of 2000, 2005, 2010 and 2014 were acquired through the U.S. Geological Survey (USGS) Earth Explorer (https://earthexplorer.usgs.gov/) (Table 1). Landsat-5 was launched by National Aeronautics and Space Administration (NASA) on March 1, 1984. It has delivered high-quality, global data of Earth's land

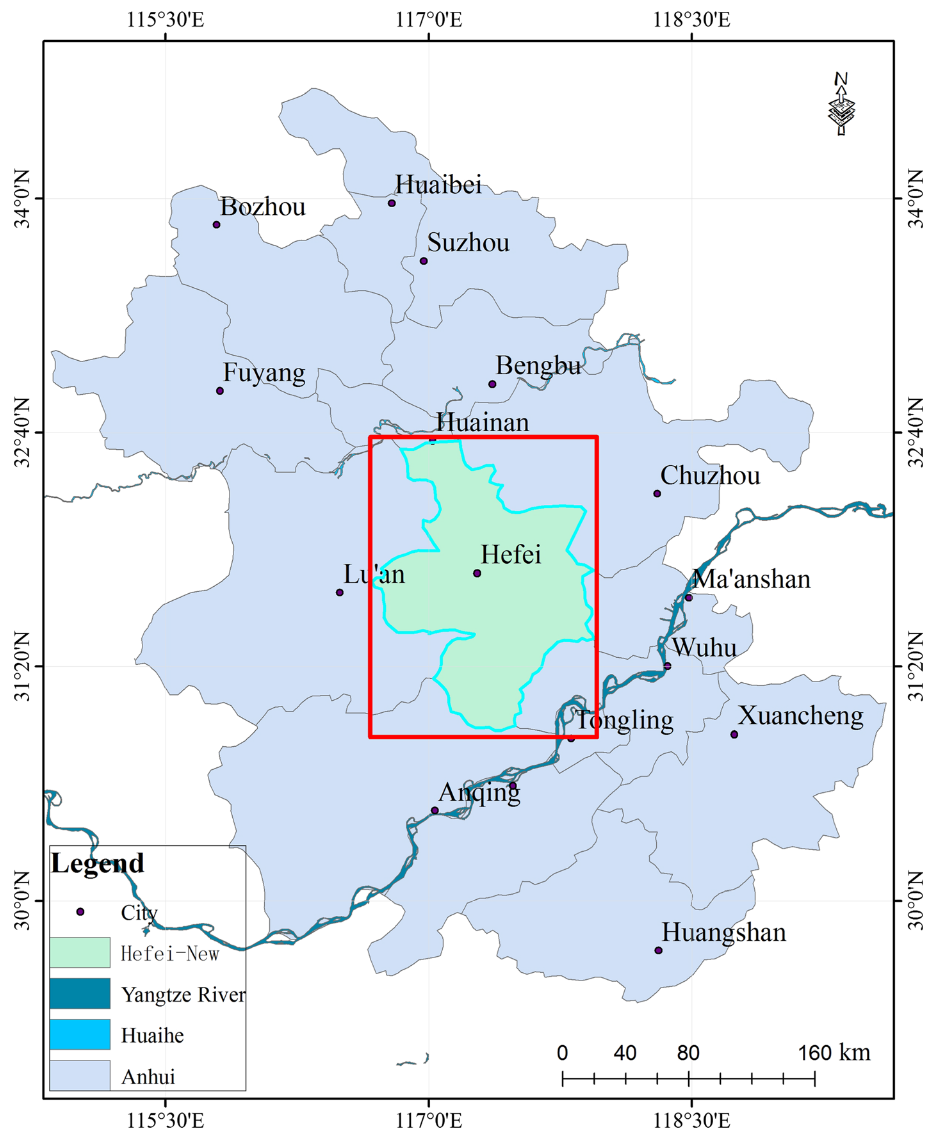

Fig. 1 Geographic location map of the study area

surface for 28 years and 10 months. In November 2011, the Thematic Mapper (TM) instrument stopped acquiring images due to a rapidly degrading electronic component. Landsat-8, as NASA′s eighth satellite in the Landsat series, was successfully launched on February 11, 2013. It carries two instruments: The Operational Land Imager (OLI) sensor owing eight multispectral bands with a spatial resolution of 30 m and the Thermal Infrared Sensor (TIRS) sensor with a spatial resolution of 100 m. Here, the Landsat-8 OLI images were used to identify the land cover types. The radiometric correction (radiometric calibration and atmospheric correction) and geometric correction were performed in the ENVI (The Environment for Visualizing Images) platform. The Fast Line-of-sight Atmospheric Analysis of Hypercubes (FLAASH) module was used to finish the radiometric correction by the UNKONWN-MSI sensor type, the attached header file (MTL.txt) and spectral response function (SRF) (Zhao et al. 2017). The geometric correction was carried out by the second-order polynomial and the nearest neighbor resampling method to ensure that the accuracy was better than 0.5 pixel.

Nearest-Neighbor Classification

The NN classification is similar to the traditional pixel-based classification process (Böhm and Krebs 2004; Jensen and Cornelis 2011). It decides which type an object belongs to in the image to be classified, based on a selection of typical ground samples and the calculation of the nearest features in the feature space. Its main classification processes can be divided into three steps. The first step is to select representative ground-truth samples of specific classes. Then, the feature space for classification can be generated by calculating the feature center of each class.

Table 1 Parameters for Landsat-5 TM and Landsat-8 OLI sensors

Acquisition date	Sensor	Band/wavelength range (μm)	Resolution (m)	Revisit period (day)	Swath (km)
April 8, 2000	TM	Band 1—Blue/0.45–0.52	30	16	185
September 15, 2000		Band 2—Green/0.52–0.60	30		
November 2, 2000		Band 3—Red/0.63–0.69	30		
May 24, 2005		Band 4—Near infrared (NIR)/0.76–0.90	30		
August 12, 2005		Band 5—Shortwave infrared (SWIR) 1/1.55–1.75	30		
January 14, 2010		Band 6—Long wave infrared (LWIR)/10.41–12.5	120		
October 29, 2010		Band 7—SWIR 2/2.08–2.35	30		
May 1, 2014	OLI	Band 1—Coastal aerosol/0.43–0.45	30	16	185
October 24, 2014		Band 2—Blue/0.45–0.51	30		
December 27, 2014		Band 3—Green/0.53–0.59	30		
		Band 4—Red/0.64–0.67	30		
		Band 5—NIR/0.85–0.88	30		
		Band 6—SWIR 1/1.57–1.65	30		
		Band 7—SWIR 2/2.11–2.29	30		
		Band 8—Panchromatic/0.50–0.68	15		
		Band 9—Cirrus/1.36–1.38	30		

Finally, the distance between the features of the unclassified classes and the statistical features of the selected samples are calculated. If the distance between the samples of the ground-truth classes is close, the unclassified pixels will be classified into a particular class. The calculation formula is shown as follows:

$$d = \sqrt{\sum_f \left| \frac{v_f^s - v_f^o}{\sigma_f} \right|} \quad (1)$$

where d represents the distance between the ground-truth sample s and the class o to be classified; v_f^s represents the eigenvalue f of the typical ground-truth samples; v_f^o represents the eigenvalue f of the pixels to be classified; and σ_f is the standard deviation of the feature f.

SEaTH Algorithm

An automatic methodology called SEaTH tool was adopted in the feature selection to seek the significant features of optimal class separation (Nussbaum et al. 2006). It combines the current status of object-oriented classification techniques commonly used in high-spatial-resolution remote sensing images, which can solve the problems faced by the object-oriented feature selection process. The basic principle of the SEaTH algorithm is divided into two parts: feature preference and threshold determination.

1. Feature preference

The automatic feature preference is based on the eigenvalue between typical ground class samples. Corresponding algorithms use the degree of separation to determine the correlation between two ground classes. The previous studies have shown that JM distance is superior to Euclidean distance or divergence (Murakami et al. 2001; Hao et al. 2014). JM distance behaves much more like probability of correct classification. Here, it was used to perform the spectral separability measures as shown in Eq. (2):

$$\mathrm{JM}(C_1,\ C_2) = \int_x \left(\sqrt{p(x|C_1)} - \sqrt{p(x|C_2)} \right)^2 \mathrm{d}x \quad (2)$$

where x denotes the pixel to be classified and C_1 and C_2, respectively, denote the two specified classes under consideration. When the samples have a normal distribution, Eq. (2) can be changed to the following equations:

$$\mathrm{JM} = 2\left(1 - e^{-B}\right) \quad (3)$$

$$B = \frac{1}{8}(e_1 - e_2)^2 \left(\frac{2}{\delta_1^2 + \delta_2^2} \right)^{-1} + \frac{1}{2} \ln \left(\frac{\delta_1^2 + \delta_2^2}{2\delta_1 \cdot \delta_2} \right) \quad (4)$$

where B denotes the Bhattacharyya distance, e_1, e_2 and δ_1, δ_2 are, respectively, the mean and variance of classes 1 and 2. The range of the JM distance is located between [0, 2]. The closer the distance is to 2, the better the separability is (Van Niel et al. 2005).

2. Determination of threshold

In addition to the feature preference, the SEaTH algorithm can also determine the feature threshold. It can save the time of repeated tests and manually adjusting the parameters during generating the rules. Additionally, the classification efficiency can be also greatly improved. The SEaTH algorithm calculates the optimal threshold of two categories in a sample feature, according to the Gaussian probability distribution (Fig. 2 and Eq. 5):

$$p(x) = p(x|C_1)p(C_1)p(x|C_2)p(C_2) \tag{5}$$

where $p(x|C_1)$ denotes that the eigenvalue of the selected sample in C_1 is normally distributed with the mean of e_1 and the variance of δ_1^2, and similarly, $p(x|C_2)$ has the same expression.

It can be seen from Fig. 2 that the eigenvalues of the selected samples in the classes C_1 and C_2 obey a normal distribution. The intersection point of the two curves is the threshold of the wrong classification of the classes C_1 and C_2, and the minimum mixed classification (T) is the best threshold to distinguish the C_1 and C_2. The T can be calculated using Eqs. 6 and 7.

$$T = \frac{\mathrm{e}_2\delta_1^2 - \mathrm{e}_1\delta_2^2 \pm \delta_1\delta_2\sqrt{(\mathrm{e}_1 - \mathrm{e}_2)^2 + 2A\left(\delta_1^2 - \delta_2^2\right)}}{\delta_1^2 - \delta_2^2} \tag{6}$$

$$A = \ln\left(\frac{n_2}{n_1} \times \frac{\delta_1}{\delta_2}\right) \tag{7}$$

where the selected number of samples in the classes C_1 and C_2 is the n_1 and n_2, respectively.

Determination of the Classification System

According to the land cover classification scheme using the 30-m resolution remote sensing imagery and the existing land cover types of the study area (Chen et al. 2015), the classification system was categorized into the six first-class categories, including woodland, grassland, cropland, wetland, artificial surface and others, respectively. The visual performance of typical land cover types can be observed in the false-color composite image of Band 5, Band 4 and Band 3 of Landsat-8 OLI (Table 2). As shown in Table 2, the in situ investigation was also carried out by taking a photograph and collecting the position using a high-precision Global Positioning System (GPS) receiver (Trimble® Geo 7X).

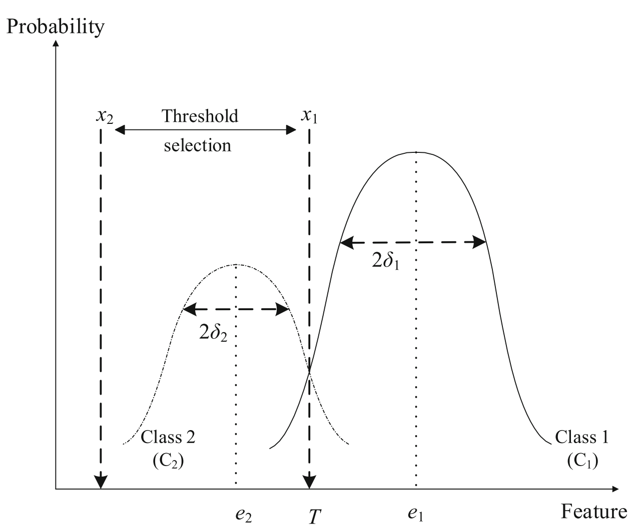

Fig. 2 A diagrammatic sketch of selecting the feature threshold

Accuracy Assessment

It is of great significance to evaluate the classification effect derived from the remotely sensed imagery. The generalized confusion matrix is appropriate for both traditional classification algorithms and sub-pixel area estimation models (Lewis and Brown 2001). The confusion matrix is usually constructed in a two-dimensional table (Fig. 3) in which the rows indicate the land cover categories determined by a classification technique, the columns indicate the same categories as identified in ground survey, and the cell values indicate the number of observations allocated to each combination of categories (Hay 1988). The confusion matrix, in our study, was generated in the ENVI where columns represent true classes, while rows represent the classifier's predictions. All the correct classifications can be found along the upper-left to lower-right diagonal. The four indicators can be generated: overall accuracy (OA), user's accuracy (UA), producer's accuracy (PA) and Kappa coefficient (k) (Congalton et al. 1983; Lewis and Brown 2001).

where i is the class number, N is the total number of classified values compared to the truth values, $p_{i,i}$ is the number of values belonging to the truth class i that have also been classified as class i (i.e., values found along the diagonal of the confusion matrix), p_{i+} is the total number of predicted values belonging to class i, and p_{+i} is the total number of truth values belonging to class i.

Results

Hierarchical Classification Combining the NN Classification and SEaTH Algorithm

Considering the advantages and disadvantages of the NN supervised classification and SEaTH algorithm, the hierarchical classification (hereafter referred to as NN-SEaTH) was adopted. Specifically, the SEaTH algorithm was used to classify the wetland and non-wetland, and the non-wetland was further classified to the vegetation and non-vegetation according to the normalized difference vegetation index (NDVI). The fine classes with similar features were then obtained using the NN classification. When the

Table 2 Visual performance of land cover types in the standard false-color composite image

Category	Sample image	Comment
Woodland	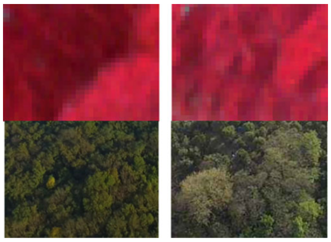	The regions are shown in dark red in the false-color composite image. They usually appear in a cluster expansion form to cover a large area
Grassland	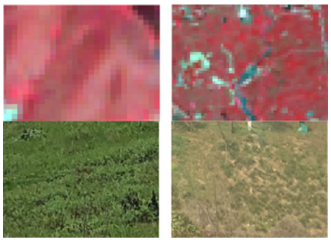	The texture is relatively smooth and mainly distributed around the woodland
Cropland	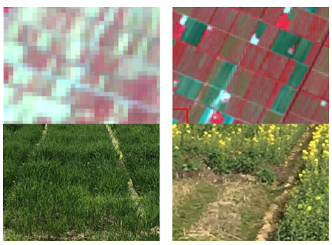	Two kinds of regions are categorized. One is the region covered by various crops (i.e., dryland, paddy field) and the other is the bare croplands (i.e., fallow land). The texture and shape of cropland are more obvious than that of bare land
Wetland	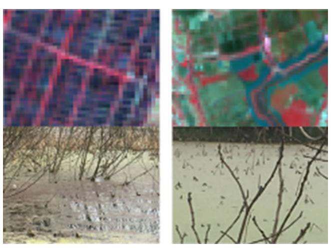	They are mainly the lakes, reservoirs, canals, rivers, flooded paddy field, etc.
Artificial surface	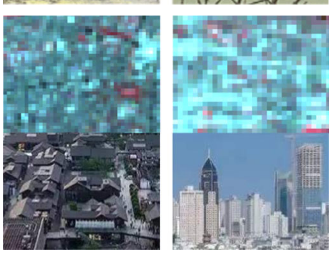	Built-up lands (residence, industrial land), mining sites and transportation lands
Others	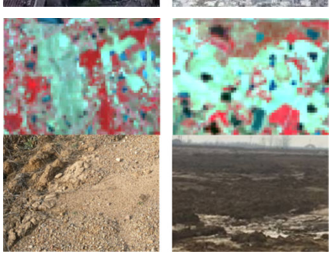	They are mainly the bare land and unused land

Fig. 3 The confusion matrix and four accuracy indicators

Truth

Predicted: Class	1	2	3	...	n	Total
1	P_{11}	P_{12}	P_{13}	...	P_{1n}	P_{1+}
2	P_{21}	P_{22}	P_{23}	...	P_{2n}	P_{2+}
3	P_{31}	P_{32}	P_{33}	...	P_{3n}	P_{3+}
...	...	...	...	...	...	...
n	P_{n1}	P_{n2}	P_{n3}	...	P_{nn}	P_{n+}
Total	P_{+1}	P_{+2}	P_{+3}	...	P_{+n}	N

$$OA=\sum_{i=1}^{n}\frac{p_{ii}}{N}$$

$$UA=\frac{p_{ii}}{p_{i+}}$$

$$PA=\frac{p_{ii}}{p_{+i}}$$

$$k=\frac{N\sum_{i=1}^{n}p_{ii}-\sum_{i=1}^{n}(p_{i+}p_{+i})}{N^2-\sum_{i=1}^{n}(p_{i+}p_{+i})}$$

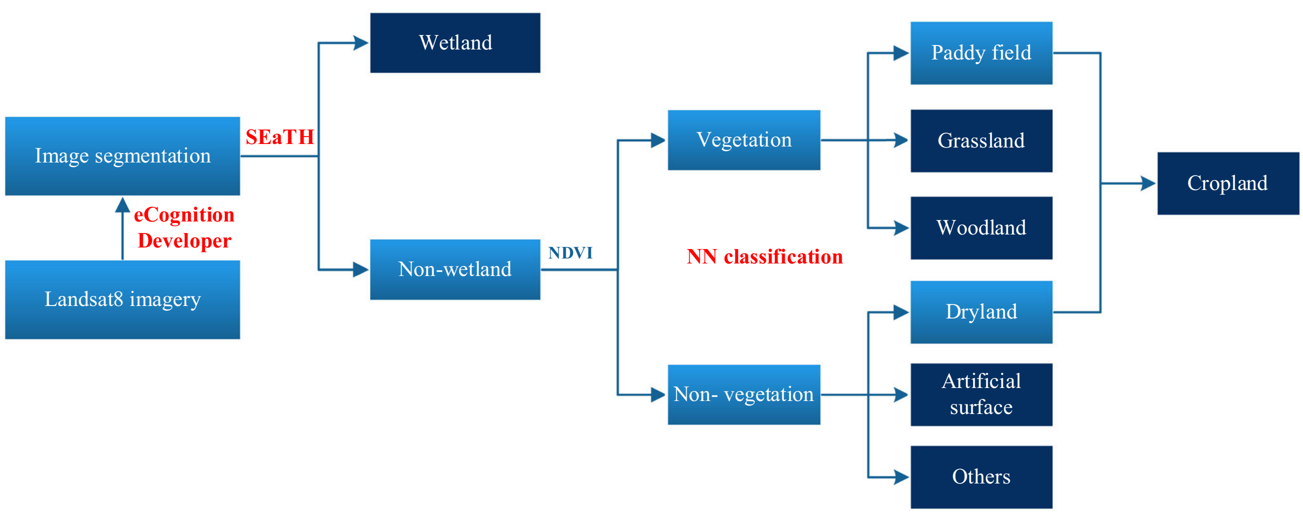

Fig. 4 The workflow of the NN-SEaTH hierarchical classification

Table 3 Feature preference and optimal threshold values

Extracted type	Background	Optimal feature	JM distance	Optimal threshold	Symbol
Wetland	Woodland	NDVI1102	2	0.113	<
		Mean0915b4	2	2390.534	<
Wetland	Grassland	NDVI1102	2	0.178	<
		Mean0915b4	2	1970.343	<
Wetland	Cropland	NDVI1102	2	0.286	<
		Mean0915b4	2	2164.831	<
Wetland	Artificial surface	NDVI1102	2	0.189	<
		Mean0915b4	2	2045.275	<

JM distance between the two land cover types was close to 2, the SEaTH algorithm can be directly applied to classify them (i.e., wetland and non-wetland). When the JM distances were not large enough (i.e., vegetation and non-vegetation), the NDVI could be used to achieve such a goal. The specific vegetation (i.e., grassland, woodland, paddy field) and non-vegetation (i.e., artificial surface, others, dryland) using NN supervised classification

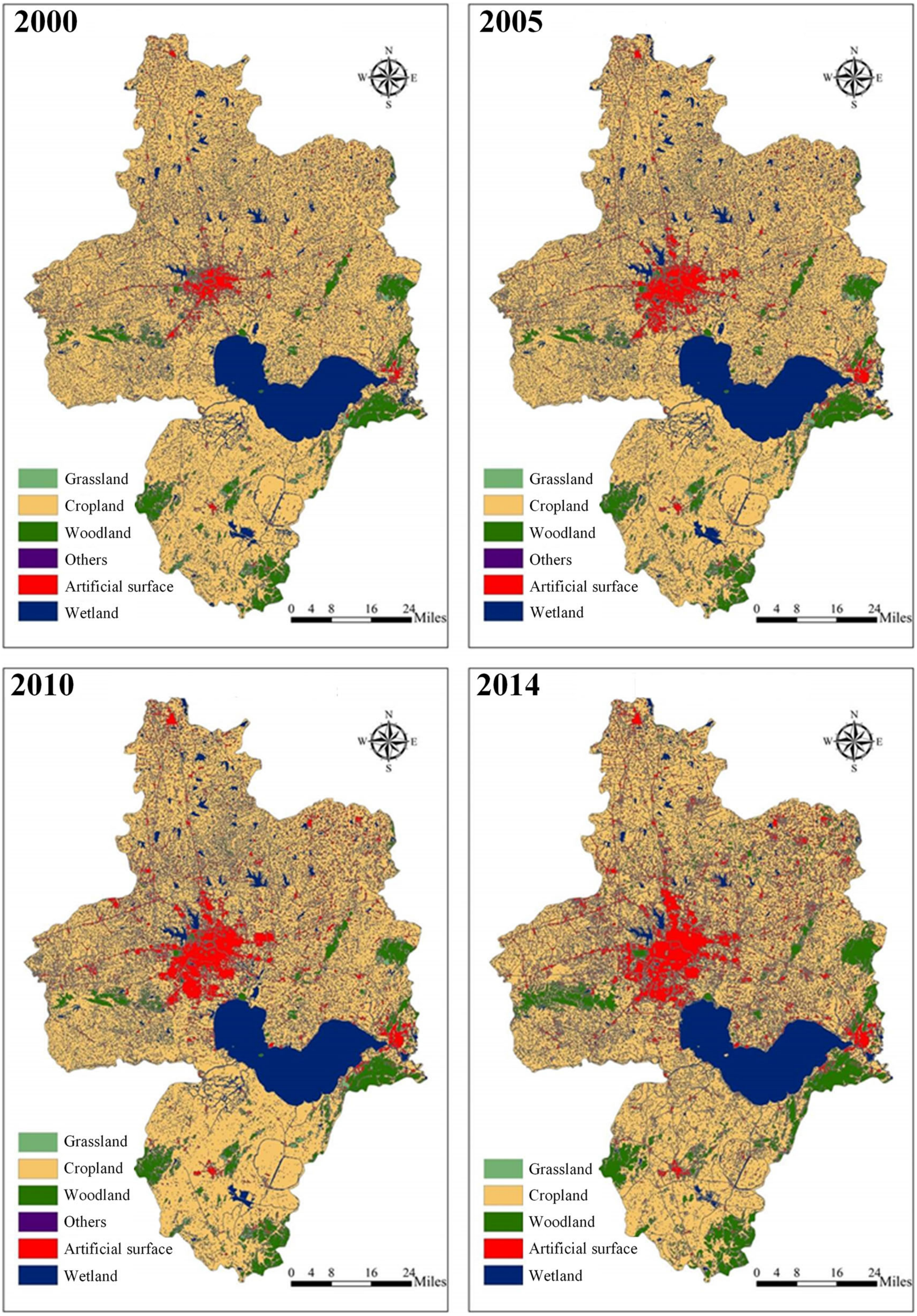

Fig. 5 Hierarchical classification results using the NN-SEaTH

method. Finally, the dryland and paddy field were combined to derive the cropland. The classification decision tree was constructed as shown in Fig. 4.

Case Study to Evaluate the NN-SEaTH

To evaluate the performance of NN-SEaTH, multitemporal Landsat-8 OLI images of Hefei were used as a case study. The image segmentation and the selection of optimized parameters were carried out in eCognition Developer. The typical samples of land cover types were selected, and then the required features could be constructed and output to a .dbf file. They were opened in Excel to statistically analyze the samples and feature values of each class by the SEaTH algorithm. The optimal feature selection and the optimal threshold could be obtained.

Specifically, the first step was to extract the wetland by the classification rules derived from the SEaTH algorithm. Multiple features must be used due to the usage of multitemporal remote sensing images in this experiment. The optimal feature might be greater than one, and only two of them needed to be selected. The principle of selection was to find the number of features appearing in the rules, which could reduce the number of rules. Since there was less bare land (others) and it was easy to identify them from the wetland, they were not involved in the calculation (Table 3). The non-wetland was then divided into vegetation and non-vegetation by using a NDVI image. Finally, the subclasses of vegetation and non-vegetation were classified by the NN classifier and corresponding feature spaces. The typical samples and feature spaces of vegetation and non-vegetation were reconstructed by the NN classifier. The features used to identify the non-vegetation were obtained as follows: shape index, GM Homo (1102b3), ratio (1102b4), ratio (0408b4) and 1102BAI, while they were the area, ratio (1102b4), shape index, GM Homo (0408b3) and GM Homo (0915b3) for identifying the three types of vegetation. Consequently, the classification results of Hefei for the 4 years of 2000, 2005, 2010 and 2014 were generated using the NN-SEaTH (Fig. 5). As a contrast, the land cover maps were also generated using the NN classifier (Fig. 6).

Accuracy Assessment

After the classification was completed, the land cover products derived from the National Remote-Sensing Investigation and Evaluation on Ecological Environment Changes during the years 2000–2010 were used to evaluate the accuracy by the confusion matrix. Additionally, a 2-m-resolution China's Gaofen-1 (GF-1) image was used to validate the land cover map of 2014. The accuracy evaluation was comparatively analyzed (Tables 4, 5, 6, 7), where C1–C6 refer to woodland, grassland, wetland, cropland, artificial surface and others, respectively.

Discussion

Comparative Analysis Between the NN and NN-SEaTH

The development of spaceborne remote sensing has facilitated the identification of land cover at different spatial scales. Several factors can affect the accuracy of remote sensing-based land cover classification, e.g., tempo-spatial resolutions of a remote sensing image, classification methods (pixel-based approaches vs object-based image analysis (OBIA)), available ancillary data, ground-truth data, etc. For example, heterogeneous spectra and similar spatial textures usually appear due to the inner complexity of land cover/use types using moderate-coarse spatial resolution remotely sensed imagery (Chen et al. 2009). It is usually difficult to accurately identify all the land cover/use types using a single classification method. In our study, freely distributed Landsat-8 OLI imagery was used to identify six first-class land cover types as many studies have reported high land cover classification accuracies when OBIA was applied to Landsat images (Phiri et al. 2018; Novelli et al. 2016; Pena et al. 2014).

The hierarchical classification is an effective alternative to improve classification accuracy. For example, a hierarchical fuzzy classification approach was proposed for high-resolution multispectral data over urban areas (Shackelford and Davis 2003). A multiclass strategy was adopted to assess the potentialities of support vector machine (SVM) classifiers in hyperdimensional feature spaces by applying binary SVMs to multiclass problems in hyperspectral data (Melgani and Bruzzone 2004). The hierarchical classification can effectively exclude the disturbance of other classes and reduce the running time for executing the classifiers.

The NN classification is simple, so it can be used to select the typical feature space in eCognition. Nevertheless, its processing speed is relatively slow, especially when the texture features are included in the feature space (Mico et al. 1996). In addition, the experimental image in this study was large, which dramatically reduced the classification efficiency. Conversely, the SEaTH algorithm has much faster running speed than that of the NN classifier. It can be used to select the optimal feature and determine the optimal threshold, but they are dependent on the JM distance. When the JM distance is greater than 1.8, the selected feature and optimal threshold are considered to be reasonable (Gao et al. 2011). The hierarchical classification combining the NN classifier and SEaTH algorithm can

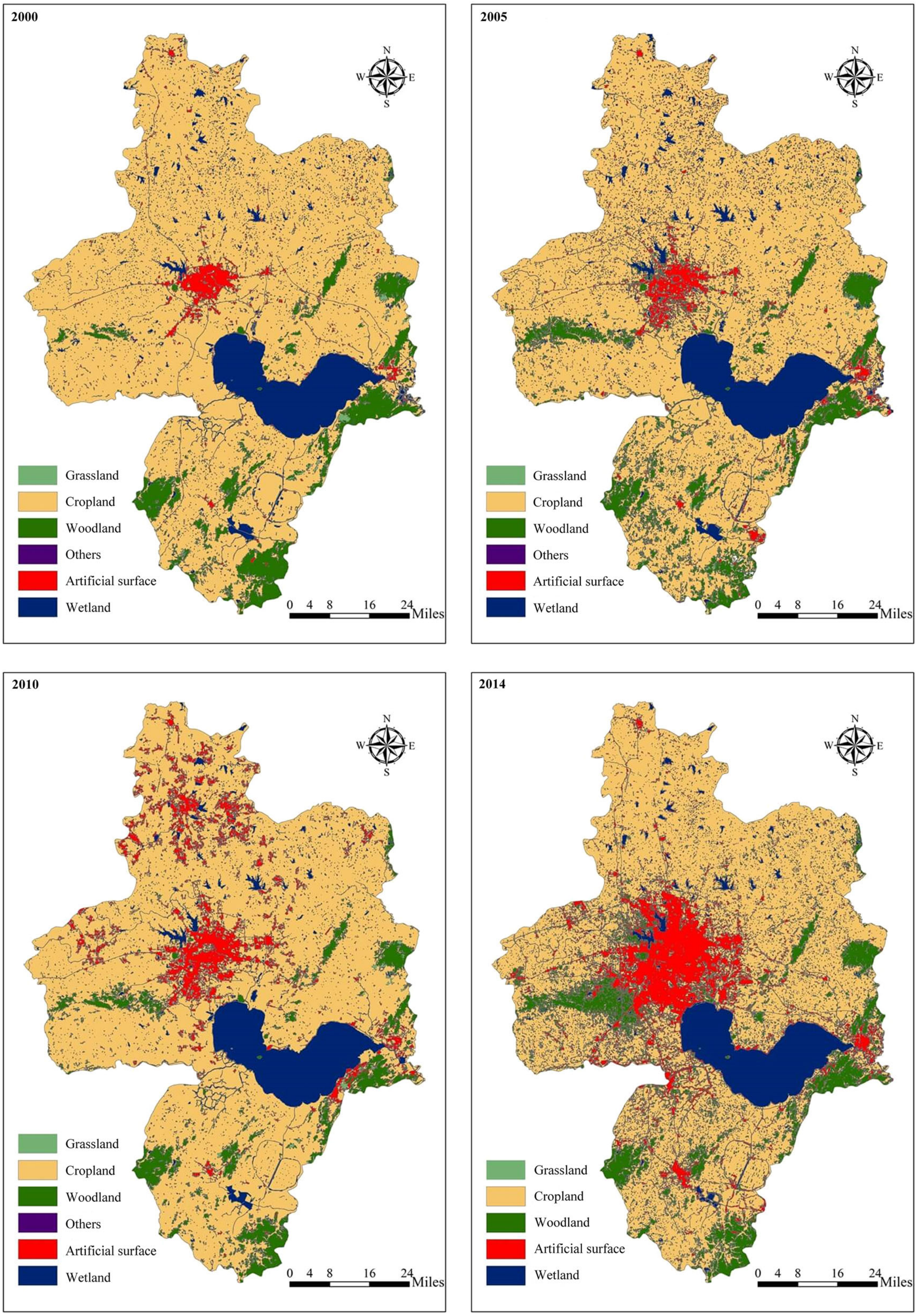

Fig. 6 The classification results using the NN classifier

Table 4 Accuracy assessment of land cover classification for the year 2000

	C1	C2	C3	C4	C5	C6
NN classification						
C1	497,003	10	19	2299	142	0
C2	46,896	53,782	6	194	0	0
C3	59	6	1,344,304	223,793	786	10
C4	175,575	575	143,605	8,208,516	594,078	249
C5	464	102	10,501	842,015	1,086,192	86
C6	0	0	43	360	0	927
UA	0.9951	0.5331	0.8586	0.8998	0.5600	0.6970
PA	0.6903	0.9873	0.8971	0.8848	0.8848	0.7288
OA	88.13%					
k	0.7503					
NN-SEaTH classification						
C1	701,856	412	920	2136	235	0
C2	14,756	52,895	1	36	17	0
C3	45	513	1,478,762	124,818	389	0
C4	9	0	15,854	8,869,461	1406	44
C5	3331	655	2941	279,943	1,144,145	26
C6	0	0	0	783	6	1202
UA	0.9948	0.7813	0.9216	0.9981	0.7995	0.6037
PA	0.9748	0.9710	0.9868	0.9561	0.9982	0.9450
OA	96.46%					
k	0.9231					

Table 5 Accuracy assessment of land cover classification of the year 2005

	C1	C2	C3	C4	C5	C6
NN classification						
C1	701,495	0	29	59	3015	0
C2	15,219	53,782	36	7	830	0
C3	17	1	1,229,372	146,356	2083	43
C4	2529	36	340,919	8,181,934	723,014	360
C5	129	0	1038	206,004	1,088,018	0
C6	0	0	10	243	92	927
UA	0.9956	0.7697	0.8922	0.8846	0.8400	0.7288
PA	0.9751	0.9993	0.7823	0.9587	0.5988	0.6970
OA	88.83%					
k	0.7660					
NN-SEaTH classification						
C1	631,593	0	892	0	0	0
C2	0	53,091	1554	0	0	0
C3	0	0	1,568,958	0	67,729	0
C4	47,059	423	0	8,321,703	24,417	0
C5	40,737	0	0	212,900	1,724,906	0
C6	0	305	0	0	0	1330
UA	0.9986	0.9716	0.9586	0.9914	0.8718	0.8135
PA	0.8780	0.9865	0.9984	0.9745	0.9493	1.00
OA	96.63%					
k	0.9269					

effectively solve the two fundamental problems in the process of conventional object-oriented classification: the focalization and sequence for different classes.

Evaluation of the Classification Accuracy

Comparing the classification results of NN and NN-SEaTH methods for the years 2000, 2005, 2010 and 2014, it can be seen that the NN-SEaTH method shows better performance than the NN classifier. More importantly, the number of missing pixels is significantly reduced. The OA and the *k* of each year have been dramatically improved, and the accuracies have been also greatly increased from the analysis of a single class. It is shown that the hierarchical classification based on the combination of the nearest-neighbor classification and SEaTH algorithm is effective in improving the classification accuracy and stability. The *k* is, respectively, 96.46%, 96.63%, 96.88%, 95.22% that are much larger than those of 88.13%, 88.83%, 88.64%, 87.33% from the NN classification approach. The *k* measures the agreement between classification and truth values, where a kappa value of 1 represents perfect agreement, while a value of 0 represents no agreement (Congalton 1991, 2001). In addition, the visual performance from the NN-SEaTH also showed better than that of the NN. For example, the regions were wetland in the northern part of land cover map of 2010 (Fig. 5), but they were wrongly classified to artificial surface in Fig. 6. The results showed that the classification accuracies have been greatly improved using the NN-SEaTH method.

It can be found that there are some differences for the UA and PA of different land cover types. In general, for the NN classification, the UA of grassland, artificial area and others are lower than other types for 2000, 2005 and 2010, most of which are less than 0.80. The PA of others is lower with the values around 0.70. Conversely, the UA of grassland is 0.8682 in 2014. We think that the imaging quality and identification performance of Landsat-8 OLI have been improved compared with Landsat-5 TM (Poursanidis et al. 2015; Rahdari 2016). In comparison with NN classification, most of the UA values of the three types have been greatly improved for the NN-SEaTH classification. The primary reason is that the six first-class land cover types are identified. It is inevitable that the commission and omission errors usually occur for each

Table 6 Accuracy assessment of land cover classification for the year 2010

	C1	C2	C3	C4	C5	C6
NN classification						
C1	701,495	0	29	59	3015	0
C2	15,219	53,782	36	7	830	0
C3	17	1	1,229,372	146,356	2083	43
C4	2529	36	340,919	8,181,934	723,014	360
C5	129	0	1038	206,004	1,088,018	0
C6	0	0	10	243	92	927
UA	0.9956	0.7697	0.8922	0.8846	0.8400	0.7288
PA	0.9751	0.9993	0.7823	0.9587	0.5988	0.6970
OA	88.64%					
k	0.7630					
NN-SEaTH classification						
C1	631,593	0	892	0	0	0
C2	0	53,091	1554	0	0	0
C3	0	0	1,568,958	0	67,729	0
C4	47,059	423	0	8,321,703	24,417	0
C5	40,737	0	0	212,900	1,724,906	0
C6	0	305	0	0	0	1330
UA	0.9986	0.9716	0.9586	0.9914	0.8718	0.8135
PA	0.8780	0.9865	0.9984	0.9745	0.9493	1.00
OA	96.88%					
k	0.9394					

Table 7 Accuracy assessment of land cover classification for the year 2014

	C1	C2	C3	C4	C5
NN classification					
C1	665,954	3639	1373	28,777	7444
C2	10,338	46,720	50	2668	719
C3	1492	97	1,286,479	206,440	15,570
C4	36,322	3220	264,255	8,088,138	797,142
C5	4438	139	18,818	203,585	995,623
UA	0.9268	0.8682	0.8189	0.9482	0.5481
PA	0.9417	0.7723	0.8519	0.8802	0.8143
OA	87.33%				
k	0.7371				
NN-SEaTH classification					
C1	628,068	1647	0	0	0
C2	0	52,168	0	3350	0
C3	12,543	0	1,419,347	76,734	5590
C4	77,933	0	79,846	8,309,132	137,280
C5	0	0	71,782	140,392	1,673,638
UA	0.9973	0.9397	0.9373	0.9657	0.8875
PA	0.8741	0.9694	0.9035	0.9742	0.9213
OA	95.22%				
k	0.9239				

category. In compassion with grassland, wetland, artificial area and others, woodland and cropland have more obvious texture and shape features, so they have higher classification accuracies. There are more heterogeneities and fragmentations for wetland, artificial area and others that are more easily affected by human activities (Goldewijk and Ramankutty 2004; Carey and Fulweiler 2012). Additionally, we think that the classification system is another essential factor affecting the classification (Cai et al. 2018; Bradter et al. 2020). It is extremely necessary that the specific and unique classification system for a certain land cover or different classes must be adapted to the study area according to the available remotely sensed imagery.

Conclusions

Land cover is a crucial approach for providing a knowledge of land management and land planning for human beings. The development of remote sensing can provide available remotely sensed imagery for land cover classification and mapping data sources of various tempo-spatial resolutions. Nevertheless, the classification algorithms and methods should be paid more attention to improve the OA, UA, PA and *k*. Although dozens of classifiers have been generated to adapt to various remote sensing images, the classification strategies are more significant to combine or merge different classifiers (i.e., hierarchical classification or stratified feature extraction). In this study, the NN classifier and SEaTH algorithm are combined to greatly improve the classification accuracy compared with the NN classifier. The study can provide a methodological reference for medium-resolution-based land cover mapping by a hierarchical classification.

Acknowledgements The project was supported by the National Natural Science Foundation of China (41601466, 61672032), the Youth Innovation Promotion Association CAS (2017085), Natural Science Research Project of Anhui Provincial Education Department (KJ2018A0009) and Anhui Provincial Science and Technology Project (17030701062).

References

Bartholome, E., & Belward, A. S. (2005). GLC2000: a new approach to global land cover mapping from Earth observation data. *International Journal of Remote Sensing, 26*(9), 1959–1977.

Böhm, C., & Krebs, F. (2004). The k-nearest neighbour join: Turbo charging the KDD process. *Knowledge and Information Systems, 6*(6), 728–749.

Bradter, U., Oconnell, J., Kunin, W. E., Boffey, C. W., Ellis, R. J., & Benton, T. G. (2020). Classifying grass-dominated habitats from remotely sensed data: The influence of spectral resolution, acquisition time and the vegetation classification system on accuracy and thematic resolution. *Science of the Total Environment, 711,* 134584.

Cai, Y., Guan, K., Peng, J., Wang, S., Seifert, C. A., Wardlow, B. D., et al. (2018). A high-performance and in-season classification system of field-level crop types using time-series Landsat data and a machine learning approach. *Remote Sensing of Environment, 210,* 35–47.

Carey, J. C., & Fulweiler, R. W. (2012). Human activities directly alter watershed dissolved silica fluxes. *Biogeochemistry, 111*(1), 125–138.

Chen, J., Ban, Y., & Li, S. (2014). China: Open access to earth land-cover map. *Nature, 514*(7523), 434.

Chen, J., Chen, J., Liao, A., Cao, X., Chen, L., Chen, X., et al. (2015). Global land cover mapping at 30 m resolution: A POK-based operational approach. *ISPRS Journal of Photogrammetry and Remote Sensing, 103*(103), 7–27.

Chen, Y., Su, W., Li, J., & Sun, Z. (2009). Hierarchical object oriented classification using very high resolution imagery and LIDAR data over urban areas. *Advances in Space Research, 43*(7), 1101–1110.

Congalton, R. G. (1991). A review of assessing the accuracy of classifications of remotely sensed data. *Remote Sensing of Environment, 37*(1), 35–46.

Congalton, R. G. (2001). Accuracy assessment and validation of remotely sensed and other spatial information. *International Journal of Wildland Fire, 10*(4), 321–328.

Congalton, R. G., Oderwald, R. G., & Mead, R. A. (1983). Assessing Landsat classification accuracy using discrete multivariate analysis statistical techniques. *Photogrammetric Engineering and Remote Sensing, 49*(12), 1671–1678.

Foley, J. A., Defries, R. S., Asner, G. P., Barford, C. C., Bonan, G. B., Carpenter, S. R., et al. (2005). Global consequences of land use. *Science, 309*(5734), 570–574.

Friedl, M. A., Mciver, D. K., Hodges, J. C., Zhang, X., Muchoney, D., Strahler, A. H., et al. (2002). Global land cover mapping from MODIS: Algorithms and early results. *Remote Sensing of Environment, 83*(1), 287–302.

Gao, Y., Marpu, P. R., Niemeyer, I., Runfola, D. M., Giner, N. M., Hamill, T., et al. (2011). Object-based classification with features extracted by a semi-automatic feature extraction algorithm-SEaTH. *Geocarto International, 26*(3), 211–226.

Goldewijk, K. K., & Ramankutty, N. (2004). Land cover change over the last three centuries due to human activities: The availability of new global data sets. *GeoJournal, 61*(4), 335–344.

Gu, X. F., & Tong, X. D. (2015). Overview of China earth observation satellite programs [space agencies]. *IEEE Geoscience and Remote Sensing Magazine, 3*(3), 113–129.

Hao, P., Wang, L., Niu, Z., Aablikim, A., Huang, N., Xu, S., et al. (2014). The potential of time series merged from Landsat-5 TM and HJ-1 CCD for crop classification: A case study for Bole and Manas counties in Xinjiang, China. *Remote Sensing, 6*(8), 7610–7631.

Hay, A. M. (1988). The derivation of global estimates from a confusion matrix. *International Journal of Remote Sensing, 9*(8), 1395–1398.

Jensen, R., & Cornelis, C. (2011). Fuzzy-rough nearest neighbour classification and prediction. *Theoretical Computer Science, 412*(42), 5871–5884.

Lambin, E. F., Turner, B., Geist, H. J., Agbola, S. B., Angelsen, A., Bruce, J. W., et al. (2001). The causes of land-use and land-cover change: Moving beyond the myths. *Global Environmental Change-Human and Policy Dimensions, 11*(4), 261–269.

Lewis, H. G., & Brown, M. (2001). A generalized confusion matrix for assessing area estimates from remotely sensed data. *International Journal of Remote Sensing, 22*(16), 22:3223–22:3235.

Loveland, T. R., Reed, B. C., Brown, J. F., Ohlen, D. O., Zhu, Z., Yang, L., et al. (2000). Development of a global land cover characteristics database and IGBP DISCover from 1 km AVHRR data. *International Journal of Remote Sensing, 21*(67), 1303–1330.

Melgani, F., & Bruzzone, L. (2004). Classification of hyperspectral remote sensing images with support vector machines. *IEEE Transactions on Geoscience and Remote Sensing, 42*(8), 1778–1790.

Mico, L., Oncina, J., & Carrasco, R. C. (1996). A fast branch & bound nearest neighbour classifier in metric spaces. *Pattern Recognition Letters, 17*(7), 731–739.

Murakami, T., Ogawa, S., Ishitsuka, N., Kumagai, K., & Saito, G. (2001). Crop discrimination with multitemporal SPOT/HRV data in the Saga Plains, Japan. *International Journal of Remote Sensing, 22*(7), 1335–1348.

Novelli, A., Aguilar, M. A., Nemmaoui, A., Aguilar, F. J., & Tarantino, E. (2016). Performance evaluation of object based greenhouse detection from Sentinel-2 MSI and Landsat 8 OLI data: A case study from Almería (Spain). *International Journal of Applied Earth Observation and Geoinformation, 52,* 403–411.

Nussbaum, S., Niemeyer, I., Canty, & M. J. (2006). SEaTH—A new tool for automated feature extraction in the context of object-oriented image analysis. In *Proceedings of the 1st International Conference on Object-based Image Analysis*, ISPRS Volume No. XXXVI 4/C42, Salzburg, Austria.

Pena, J. M., Gutierrez, P. A., Hervasmartinez, C., Six, J., Plant, R. E., & Lopezgranados, F. (2014). Object-based image classification of summer crops with machine learning methods. *Remote Sensing, 6*(6), 5019–5041.

Phiri, D., Morgenroth, J., Xu, C., & Hermosilla, T. (2018). Effects of pre-processing methods on Landsat OLI-8 land cover classification using OBIA and random forests classifier. *International Journal of Applied Earth Observation and Geoinformation, 73,* 170–178.

Poursanidis, D., Chrysoulakis, N., & Mitraka, Z. (2015). Landsat 8 vs. Landsat 5: A comparison based on urban and peri-urban land cover mapping. *International Journal of Applied Earth Observation and Geoinformation, 35*(35), 259–269.

Rahdari, V. (2016). Comparison of OLI and TM multi-spectral satellite imagery land-use and land-cover mapping using hierarchical concept of Earth surface matrix. *Computer Engineering and Intelligent Systems, 7*(10), 26–36.

Searchinger, T., Heimlich, R., Houghton, R. A., Dong, F., Elobeid, A., Fabiosa, J., et al. (2008). Use of US croplands for biofuels increases greenhouse gases through emissions from land-use change. *Science, 319,* 1238–1240.

Seto, K. C., & Fragkias, M. (2005). Quantifying spatiotemporal patterns of urban land-use change in four cities of China with time series landscape metrics. *Landscape Ecology, 20*(7), 871–888.

Shackelford, A. K., & Davis, C. H. (2003). A hierarchical fuzzy classification approach for high-resolution multispectral data over urban areas. *IEEE Transactions on Geoscience and Remote Sensing, 41*(9), 1920–1932.

Singh, P. P., & Garg, R. D. (2011). Land use and land cover classification using Satellite Imagery: A hybrid classifier and neural network approach. In *Proceedings of the first International Conference on Advances in Modeling, Optimization and Computing* (pp. 753–762). Roorkee, India.

Singh, P. P., & Garg, R. D. (2014). Classification of high resolution satellite images using spatial constraints-based fuzzy clustering. *Journal of Applied Remote Sensing, 8*(1), 083526.

Singh, P. P., & Garg, R. D. (2015). Fixed point ICA based approach for maximizing the non-Gaussianity in remote sensing image classification. *Journal of The Indian Society of Remote Sensing, 43*(4), 851–858.

Singh, P. P., & Garg, R. D. (2016). On sphering the high resolution satellite image using fixed point based ICA approach. In *Proceedings of the first international conference on Computer Vision and Image Processing* (pp. 411–419). Roorkee, India.

Tong, S. T., & Chen, W. (2002). Modeling the relationship between land use and surface water quality. *Journal of Environmental Management, 66*(4), 377–393.

Van Niel, T. G., Mcvicar, T. R., & Datt, B. (2005). On the relationship between training sample size and data dimensionality: Monte Carlo analysis of broadband multi-temporal classification. *Remote Sensing of Environment, 98*(4), 468–480.

Zhao, J., Huang, L., Yang, H., Zhang, D., & Dong, L. (2017). Evaluation of Landsat-8 OLI satellite imagery by a cross-comparison method combining spectral and texture features. *Journal of Optics, 46*(3), 295–303.